Expert Systems with Applications 41 (2014) 2595–2607

Contents lists available at ScienceDirect

Expert Systems with Applications

journal homepage: www.elsevier.com/locate/eswa

Integrated modeling and analysis of dynamics for electric vehicle powertrains

Gwangmin Park [a], Seonghun Lee [b], Sungho Jin [b], Sangshin Kwak [c,*]

[a] Daegu-Gyeongbuk Regional Division, Korea Automotive Technology Institute, Daegu, Republic of Korea
[b] Robotics Research Division, Daegu Gyeongbuk Institute of Science & Technology, Daegu, Republic of Korea
[c] School of Electrical and Electronics Engineering, Chung-ang University, 221 Heukseok-dong, Dongjak-gu, Seoul 156-756, Republic of Korea

ARTICLE INFO

Keywords:
Electric vehicles
Powertrains
Analytic modeling
Dynamics of vehicles

ABSTRACT

Powertrain of an electric vehicle (EV) is a compound system with an electrical sub-system, such as batteries, inverters, and electrical motors, as well as a mechanical sub-system, including transmissions, differential, and wheels. Since the electrical systems directly affect the vehicle driving performance and dynamics of an EV, integrated modeling considering both the mechanical and electrical systems is essential to assess ultimate kinetic and dynamic characteristics of an EV in terms of input electrical quantities. In this paper, an entire analytic model for the powertrain of EVs is developed to describe EV dynamics with respect to electrical signals, in consideration of both mechanical and electrical systems. Theoretical models based on mathematical expressions, combining the mechanical power system and the electrical power systems, are derived for predicting the final vehicle driving performance as a function of electrical quantities. In addition, a Matlab model of an EV is developed to verify the derived mathematical analysis model. Based on the theoretical model of the powertrain, a variety of relationships between electrical quantities and vehicle dynamics, such as velocity, acceleration, and forces of the EVs, are finally investigated and analyzed.

1. Introduction

Recent issues of exhausting fossil fuels and global warming caused by internal combustion engine (ICE) vehicles have led to considerable efforts to develop EVs as environment-friendly vehicles utilizing electrical energy sources (Butler, Ehsani, & Kamath, 1999; García, Torreglosa, Fernández, & Jurado, 2013). There is a large difference between the drivetrain system of EVs and ICE vehicles. In contrast with conventional ICE vehicles, the powertrain systems of EVs run electric motors through electrical energy stored in batteries. Accordingly, EVs are equipped with power electronics circuits, such as DC–DC converters and DC–AC inverters. Permanent magnet synchronous motors (PMSMs) applied to EVs has recently become more common, due to their various advantages, such as light weight, easy control, high power factor, and high torque density. In particular, interior PMSMs of compact size, high efficiency and with small torque ripples, have been commonly used for EVs (Murakami, Kataoka, Honda, Morimoto, & Takeda, 2001; Na, Park, Kim, & Kwak, 2011). Electrical energy is transformed to mechanical energy through the electrical motors, in order to provide mechanical power to drive the wheels. Since the powertrain system of an EV is a complex system with both the electrical and the mechanical sub-systems, it is necessary to model and analyze the powertrain systems of the EV in consideration of the two sub-systems, to clearly address the vehicle dynamics. In particular, integrated modeling and analysis of the entire EV powertrain system is required to discover how a variety of vehicle dynamic characteristics are related with electrical quantities (Gao, Mi, & Emadi, 2007). However, analytic studies on EV powertrains have been mostly focused on modeling and analysis of mechanical power system without taking electrical systems into consideration (Ehsani, Rahman, & Toliyat, 1997; Kroeze & Krein, 2008; Mapelli, Tarsitano, & Mauri, 2010; Nair & Rajagopal, 2010; Onoda & Emadi, 2004; Powell, Bailey, & Cikanek, 1998). Systematic analysis integrating the electrical and the mechanical sub-systems until now have been missing in the literature. Generic EV models have been designed by utilizing computer-aided simulation tools, such as Matlab/Simulink without deriving mathematical analysis (Kroeze & Krein, 2008; Nair & Rajagopal, 2010). Some theoretical analyses of EV powertrains have been, without investigating explicit correlations between vehicle dynamics and electrical quantities, implemented based on models for mechanical components (Ehsani et al., 1997; Mapelli et al., 2010; Powell et al., 1998).

This paper constructs behavior models based on mathematical approaches for respective electrical and mechanical sub-systems. With numerical analysis for the two sub-systems, integrated analytic expressions combining the two sub-systems are, through

* Corresponding author. Tel.: +82 2 820 5346; fax: +82 2 825 1584.
E-mail address: sskwak@cau.ac.kr (S. Kwak).

0957-4174/$ - see front matter © 2013 Elsevier Ltd. All rights reserved.
http://dx.doi.org/10.1016/j.eswa.2013.10.007

theoretical derivations, derived to obtain theoretical closed-form expressions. The theoretical model constructed in this paper can describe evident relationships between electrical quantities and vehicle dynamics such as velocity, acceleration, and forces of the EV. Having derived integrated theoretical models, the paper then constructs a Matlab/Simulink model for an entire EV powertrain to validate the developed mathematical analysis models. Confirming that the results from the two models are consistent for a standard vehicle speed profile, a variety of influences on vehicle dynamics, including velocity, acceleration, and forces of the EV, of electrical quantities are, in detail, presented and analyzed in this paper. The scientific innovation of this paper is developing the generic EV model based on detailed and accurate analytic models with the correlation between the electric input signals and the mechanical final output variables, which has not been covered in existing research. With theoretical analysis for respective electrical and mechanical sub-systems, integrated models of the EV powertrain with the PMSM type are derived by combining the two subsystems through mathematical derivations. Furthermore, the derived analytic models have been validated, in comparison with the simulation model developed with the Matlab/Simulink libraries, by testing with the FTP-75 driving cycle. The developed analysis models directly relates the dynamic vehicle behaviors with the electrical signals, including the motor phase currents and the angular rotor speed, which are already measured by the electrical sensors and realized for the motor controls of the EV powertrains. As a result, final EV dynamics, such as the wheel speed, the wheel torque, the vertical forces on front and rear wheel, the tractive force, and the speed/acceleration in the vehicle tractive direction, can be easily monitored and predicted using the proposed analysis models and the real-time electric signals.

2. Modeling of an electric vehicle powertrain

Depending on the mechanical structures as well as the number of motors, and, EV powertrain systems can be generally classified into six possible configurations, as illustrated in Fig. 1. According to the number of motors employed in the drivetrains, the six arrangements of the EV powertrains in Fig. 1 can be categorized with two classes: one-motor and two-motor based powertrains, which are summarized in Table 1.

Fig. 1(a)–(c) illustrate one-motor based EV powertrains, where single motor delivers driving power to wheels through mechanical constituents. The one-motor based EV powertrains have been favored, since they can maximize the utilization of existing mechanical systems in conventional ICE vehicles. As a result, the EV driveling configurations with one-motor based structure have been mostly employed for EV systems due to their structural similarity with the ICE vehicles. The differentials splitting generated torque to the wheels are essential, which enables the wheels to be driven at different speeds when vehicles turn corners (Chan, 2002). The two-motor based EV powertrains can shorten mechanical transmission paths from the electric motor to the driving wheel, as shown in Fig. 1(d)–(f). Individual motors with dedicated converters are used to provide speed and toque for respective wheels, which results in no requirements for differentials. Therefore, simplified structures in mechanical systems of the two-motor based EV drivelines are obtained at the cost of increased complexity of electrical components and controllers. The one-motor based EV drivelines have mostly been adopted in commercial EVs, while the two-motor based powertrains have been utilized for small-scale demonstrations. Thus, this paper deals with modeling and analysis of the one-motor based EV system.

The entire powertrain of the EVs shown as Fig. 1(a) is, in detail, represented in Fig. 2 with the both electrical and mechanical sub-systems, in the direction of power transmission. The electrical sub-system consists of electronic controller, power converters including a DC–AC inverter and DC–DC converter, batteries, and a PMSM. Speed profiles are obtained by driver's commands resulted from the brake and accelerator pedals operated by drivers. The speed profiles of the EVs are converted to the speed command and the torque command of the electrical motor. The electronic controller generates gating signals of the inverter to control desired speed and torque of the motor, by adjusting the magnitude and the frequency of the currents through the motor. The electrical power of the PMSM controlled by the power converter is delivered to the mechanical system via the clutch, which links the electrical and the mechanical sub-systems. The mechanical sub-system is comprised of a clutch, gearbox (transmission), differential, axle shaft, and wheels for generating driving force. Through all the mechanical constituents, final EV dynamic outputs are created as forms of a tractive force F_x, a vertical force F_z of vehicles, a vehicle speed v_x, and a vehicle acceleration a_x. Due to the direct coupling of the two sub-systems and the sequential power transmission in EVs, an integrated electro-mechanical model combining the electrical and the mechanical sub-systems enables the eventual vehicle

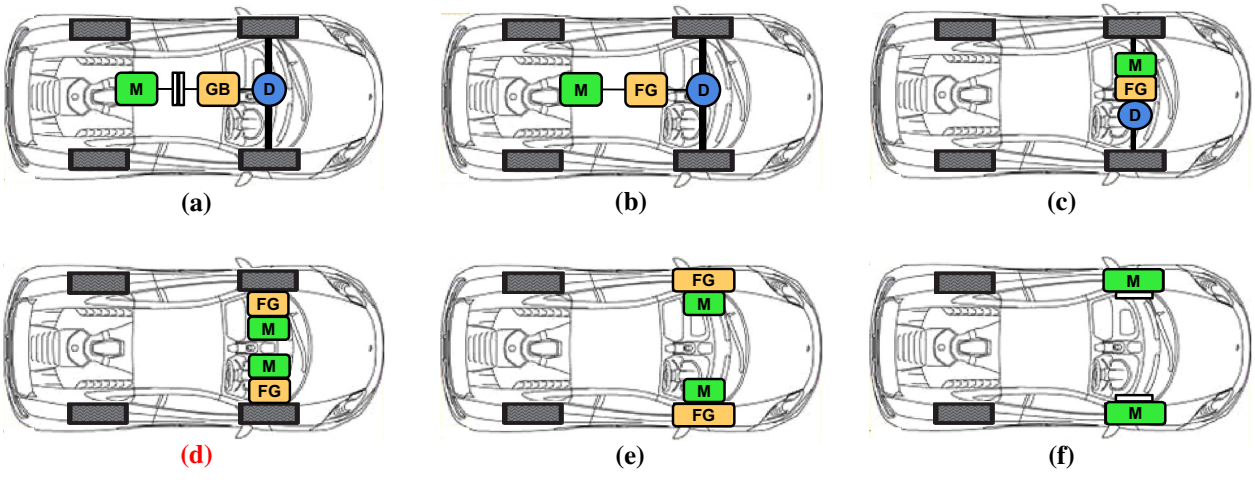

Fig. 1. Six types of EV configurations. One-motor based EV powertrains: (a) Conventional. (b) No transmission (RF). (c) No transmission (FF). Two-motor based EV powertrains: (d) No differential. (e) In-wheel with FG. (f) In-wheel without FG.

Table 1
Categories of EV powertrain structures.

One-motor based EV powertrains	Two-motor based EV powertrains
(a) Conventional type: The EV propulsion system consists of a differential (D), a gearbox (GB), a clutch (C), and an electric motor (M). This configuration can be considered as a counterpart of an ICE vehicle with rear-engine-front-wheel drive, where the ICE is replaced by an electric motor	*(d) No differential type:* Two electric motors are employed for individual front wheel to eliminate a differential. The two motors are connected to the front wheels through the mechanical fixed gearing
(b) No transmission type: Rear-engine-Front-wheel (RF) This configuration, with fixed gearing (FG) used instead of a clutch and gearbox, is quite similar as the conventional one	*(e) In wheel type with fixed gear (FG)* This type is similar to the no-differential type in (d), except different location of the electric motors. Electric motors are embedded in wheels for the in-wheel type
(c) No transmission type: Front-engine-Front-wheel (FF) The electric motor, fixed gearing, and differential are placed together in the front, just like ICE vehicles with front-engine-front-wheel drives	*(f) In wheel type without fixed gear (FG)* Mechanical gearing is completely removed for this type. The vehicle speed directly depends on the motor speed

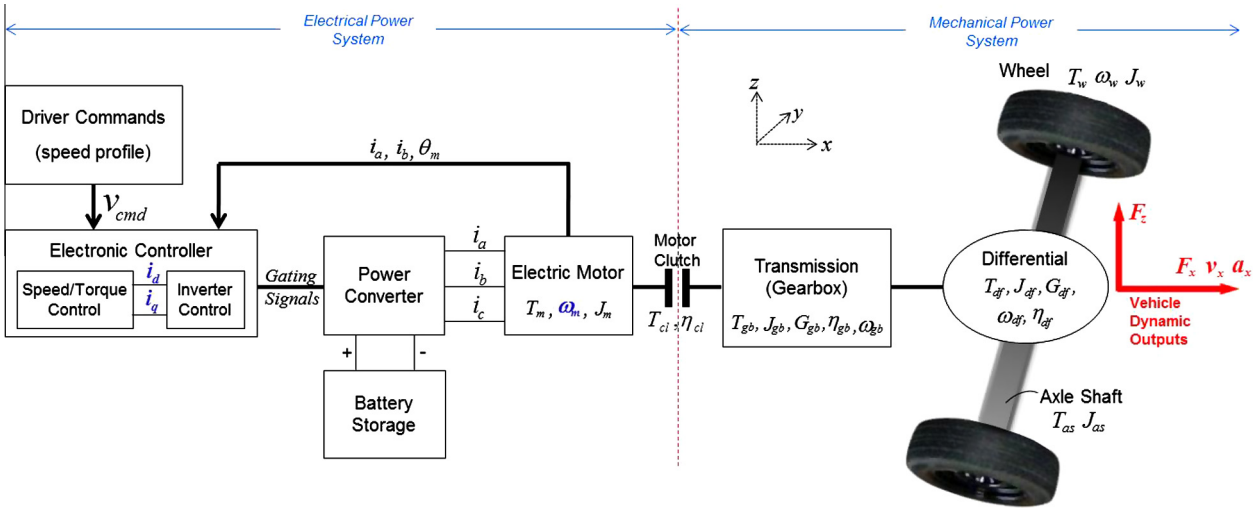

Fig. 2. Entire block diagram of conventional EV powertrain.

dynamics, including F_x, F_z, v_x, and a_x, to be expressed as a function of electrical quantities, such as the inverter output currents and torque of the PMSM. Note that the motor clutch and the transmission of Fig. 1(a) perform the same function as the fixed gearing of Fig. 1(b) and (c). Thus, model and the analysis in the EV powertrains of Fig. 1(a), which is a target of this paper, can be easily expanded into the EV drivelines of Fig. 1(b) and (c), by simply replacing the clutch and the transmission with the fixed gearing.

2.1. Behavior model of electrical system

The motor torque T_m and the motor speed ω_m, which are correspondent to output quantities of the electrical sub-system, are dependent on the controllable magnitude and the adjustable frequency of the inverter output currents, i_a, i_b, and i_c. The magnitude and the frequency commands of the inverter output currents are set by the speed and the torque control resulted in the driver's speed profile. The three-phase inverter output currents, produced by the pulsewidth modulation of the three-phase inverter, are generally dealt with the dq currents i_d and i_q in the electronic controller performing the speed and the torque control. As a result, the inverter output currents in the dq reference frame can be assumed as fundamental electrical sources in the EV powertrains, which are finally converted to the vehicle dynamic outputs.

The input currents of the PMSM in the abc reference frame can be transformed into the dq reference frame as (Kwak, 2012)

$$\begin{bmatrix} i_d \\ i_q \\ i_0 \end{bmatrix} = \frac{2}{3} \begin{bmatrix} \cos\theta_e & \cos\left(\theta_e - \frac{2\pi}{3}\right) & \cos\left(\theta_e + \frac{2\pi}{3}\right) \\ -\sin\theta_e & -\sin\left(\theta_e - \frac{2\pi}{3}\right) & -\sin\left(\theta_e + \frac{2\pi}{3}\right) \\ \frac{1}{\sqrt{2}} & \frac{1}{\sqrt{2}} & \frac{1}{\sqrt{2}} \end{bmatrix} \begin{bmatrix} i_a \\ i_b \\ i_c \end{bmatrix} \quad (1)$$

where, the electrical angular displacement of motors θ_e is given by

$$\theta_e = \frac{P}{2}\theta_m = \int \omega_e dt \quad (2)$$

where, θ_m and P denote the mechanical angular displacement of the rotor and the number of pole of the motor, respectively. In the dq reference frame, the dynamic models for the d-axis voltage v_d, the q-axis voltage v_q of the PMSM are expressed as (Mohan, Underland, & Robbins, 1995)

$$v_d = R_s i_d + \frac{d\lambda_{ds}}{dt} - \omega_r \lambda_{qs} \quad (3)$$

$$v_q = R_s i_q + \frac{d\lambda_{qs}}{dt} + \omega_r \lambda_{ds} \quad (4)$$

$$\lambda_{ds} = L_d i_d + \lambda_f, \lambda_{qs} = L_q i_q \quad (5)$$

where, R_s is the stator winding resistance, and ω_r is the electrical angular speed of the rotor, λ_{ds} and λ_{qs} are the dq-axes stator flux linkage components, respectively. In addition, L_d and L_q denote the dq-axes inductance components, and λ_f is the flux linkage due to the rotor magnets, respectively. The electromagnetic torque of the PMSM T_m is

$$T_m = \frac{3P}{4}\left[\lambda_f i_q + (L_d - L_q) i_d i_q\right]. \quad (6)$$

The mechanical dynamics of the PMSM are given by

$$J_m \frac{d\omega_m}{dt} = T_m - T_L - B_m \omega_m \ \omega_m = \left(\frac{2}{P}\right)\omega_r \quad (7)$$

where, ω_m is the mechanical angular speed of the rotor, simply referred to as the rotor speed. Furthermore, J_m, B_m, and T_L are the moment of inertia, viscous friction coefficient, and load torque, respectively.

2.2. Behavior model of mechanical system

In the mechanical sub-system of Fig. 2, the electromechanical torque of the PMSM is transmitted to the wheels of the EV with considerable reduction due to the inertia and damping of individual mechanical components. As a result, the equivalent rotational inertia J and energy transmission efficiency η of the respective mechanical components are reflected in the behavior model of mechanical sub-system (Hayes, Oliveira, Vaughan, & Egan, 2011). The energy transmission efficiency η, which indicates the energy loss due to damping and friction of each mechanical component, can be supposed to be a constant value (Mapelli et al., 2010). In case that the motor clutch is connected, the electromechanical torque T_m is converted into the output torque of the mechanical power shaft T_{cl} as

$$T_{cl} = \eta_{cl} T_m \quad (8)$$

where, η_{cl} denotes the energy transmission efficiency of the clutch. The output torques, generated from the gearbox and the differential, depend on the corresponding reduction gear ratios and damping caused by inertia. Consequently, the torque of the differential T_{df} is determined as

$$T_{df} = (\eta_{cl} T_m - J_{gb}\dot{\omega}_{gb}) G_{gb} \eta_{gb} \quad (9)$$

where, $\dot{\omega}$ and G denote the angular acceleration and the gear ratio, respectively.

The subscripts *gb* and *df* mean the parameters related to the gearbox and the differential, respectively. The output torque of the differential is delivered to the drive wheels through the axle shaft, which can be expressed as

$$T_w = T_{as} - J_{as}\dot{\omega}_{as}. \quad (10)$$

The subscripts *as* and *w* represent the parameters of the axle shaft and drive wheels, respectively. As rotational power is applied to the reduction gear devices, such as the differential and the gearbox, the angular speed and the angular acceleration are inversely proportional to the gear ratio, which can be written by

$$\dot{\omega}_{df} = \frac{\dot{\omega}_m}{G_{gb}}, \quad \dot{\omega}_{as} = \dot{\omega}_w = \frac{\dot{\omega}_{df}}{G_{df}} = \frac{\dot{\omega}_m}{G_{total}}. \quad (11)$$

where,

$$G_{total} = G_{gb} G_{df}.$$

Therefore, by substituting (8), (9), and (11) into (10), the endmost mechanical torque T_w can be derived in terms of the electrical variables of the PMSM, T_m and $\dot{\omega}_m$, as:

$$T_w = G_{total}\eta_{total} T_m J^*_{total}\dot{\omega}_m \quad (12)$$

where,

$$J^*_{total} = J_{gb} G_{total}\eta_{gb}\eta_{df} + \frac{J_{df}\eta_{df} G_{df}}{G_{gb}} + \frac{J_{as}}{G_{total}}$$

$$\eta_{total} = \eta_{cl}\eta_{gb}\eta_{df}.$$

Total rotational inertia of all the rotating mechanical elements in the powertrain, including the gearbox, the differential, the axle shaft, and the wheels, is defined with the total inertia J_{total} in (12). It should be noted that the second term in (12) represents the rotational loss in the output torque of the wheels, due to the rotational inertia of the mechanical components. From (12), it is evident that the rotational loss occurring in the mechanical sub-system increases with increasing acceleration of the PMSM. According to (12) and Newton's law for rotational motion, the tractive force of the vehicle F_x, i.e., the friction force between the tire and the road surface, can be calculated as (Fujii & Fujimoto, 2007; Gao et al., 2007; Yin, Oh, & Hori, 2009)

$$F_x = \frac{T_w}{R_w} - \frac{J_w\dot{\omega}_w}{R_w} = \frac{G_{total}\eta_{total}}{R_w} T_m - \frac{J_{total}\dot{\omega}_m}{R_w} \quad (13)$$

where,

$$\dot{\omega}_w = \frac{T_w + R_w^2 m \omega_w \dot{\lambda}}{J_w + R_w^2 m(1-\lambda)}$$

$$\lambda = \frac{v_w - v_x}{max(v_w, v_x)}$$

$$J_{total} = J^*_{total} + \frac{J_w}{G_{total}}.$$

λ, v_w, and R_w are the slip ratio, the linear speed of the wheel, and the effective radius of the drive wheels, respectively. When the slip starts to occur, the difference between the vehicle speed and the linear speed of the wheel becomes increased, which means that the acceleration of the wheel is larger than that of the vehicle. Thus, the magnitude of the wheel slip is dependent on the angular acceleration of the wheel (Yin et al., 2009). Another main factor of the friction coefficient is the road surface condition in addition to the slip ratio (Fujii & Fujimoto, 2007; Gao et al., 2007). The road surface condition is assumed as dry pavement with a high road surface adhesion coefficient in this research, in order to consider general driving condition and avoid the complicated relationship between the friction coefficient and the slip ratio (Powell et al., 1998; Yin et al., 2009). Assuming the road surface with the good adhesion, more simplified relationships can be achieved and accordingly faster execution time can be obtained, due to the linearization of a nonlinear road surface interface model. In addition, it is suitable for the general EV driving condition without severe acceleration and deceleration. However, it is required to estimate the road surface adhesion coefficient on the real-time basis for deriving very precise tractive force, because the real road surface condition varies nonlinearly. Fig. 3 illustrates an equivalent two-wheel model of vehicles, where the horizontal distances from the center of gravity (CG) of the vehicle to each wheel are represented by a_1 and a_2, respectively. On the other hand, the vertical distance from the road surface to the CG of the vehicle is denoted as h. The vertical forces

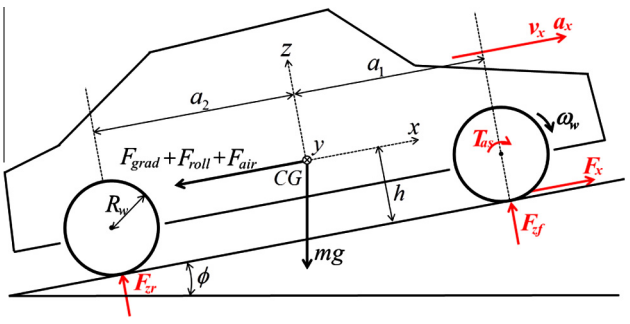

Fig. 3. Two-wheel based vehicle model.

applied to the front and the rear wheels in the two-wheel model F_{zf} and F_{zr} can be expressed as (14) and (15), respectively (Jazar, 2008)

$$F_{zf} = \frac{1}{a_1 + a_2}\left[a_2 mg\cos\phi - h\left(\frac{G_{total}\eta_{total}}{R_w}T_m - \frac{J_{total}}{R_w}\dot{\omega}_m\right)\right] \quad (14)$$

$$F_{zr} = \frac{1}{a_1 + a_2}\left[a_1 mg\cos\phi + h\left(\frac{G_{total}\eta_{total}}{R_w}T_m - \frac{J_{total}}{R_w}\dot{\omega}_m\right)\right] \quad (15)$$

where, m and ϕ imply the effective mass of the vehicle and the angle of the road, respectively. As shown in (13) and (15), the acceleration of the PMSM $\dot{\omega}_m$ associated with the total inertia J_{total} functions as an attenuating factor to reduce both the tractive force F_x and the vertical force on the rear wheel F_{zr}. On the other hand, the vertical force on the front wheel F_{zf} increases with the increasing acceleration of the PMSM. Since actual vehicle motion in the tractive direction is affected by driving resistances acting on the vehicle, the vehicle speed v_x and acceleration a_x in the tractive direction should be modeled with the effects of the resistances as well as the tractive force F_x on the vehicle. The driving resistances, as shown in Fig. 3, are composed of the gradient resistance F_{grad} generated by gradient of road surface, the rolling resistance F_{roll} caused by frictional force, and aerodynamic resistance F_{air}. The total driving forces in the tractive direction, considering the three driving resistances, can be expressed as

$$\begin{aligned}\Sigma F_x &= F_x - (F_{grad} + F_{roll} + F_{air}) \\ &= F_x - (mg\sin\phi + \mu_x mg + k_{air}v_x^2)\end{aligned} \quad (16)$$

where,

$k_{air} = 0.5 C_D \rho A.$

The coefficients of rolling resistance and aerodynamic drag are represented with μ_x and C_D, respectively. Moreover, the air density and the front projection area of the vehicle are ρ and A, respectively. Using (11), (13), and (16), the vehicle acceleration in the tractive direction a_x can be derived by

$$a_x = \left(\frac{G_{total}\eta_{total}}{R_w}T_m - mg\sin\phi - \mu_x mg - k_{air}v_x^2\right)\frac{1}{m + \Delta m} \quad (17)$$

where,

$$\Delta m = \frac{J_{total}G_{total}m}{mR_w^2 - J_w}.$$

The vehicle speed in the tractive direction v_x can be easily obtained by integrating (17) with respect to time. The tractive force and the vertical forces of the vehicles in (13)–(15) are associated with the acceleration of the PMSM $\dot{\omega}_m$. By using (11) into (17), the PMSM acceleration $\dot{\omega}_m$ can be derived as a function of the electromagnetic torque T_m, rotor speed ω_m, mechanical parameters, and vehicle parameters as

$$\dot{\omega}_m = \frac{G_{total}}{R_w(m+\Delta m)}\left(\frac{G_{total}\eta_{total}}{R_w}T_m - mg\sin\phi - \mu_x mg - k_{air}\left(\frac{\omega_m R_w}{G_{total}}\right)^2\right) \quad (18)$$

3. Integrated model of electric vehicle powertrains

3.1. Mathematical analysis models

The vehicle dynamic outputs can be clearly quantified as a function of electrical quantities using behavior models obtained from the electrical and mechanical sub-systems. The vehicle dynamics are summarized with the seven physical quantities, the wheel speed ω_w, the wheel torque T_w, the vertical forces F_{zr} and F_{zf}, the tractive force F_x, the speed v_x, and the acceleration a_x in the vehicle tractive direction. By integrating the behavior models determined in the respective electrical and mechanical sub-systems, the seven vehicle dynamic outputs describing vehicle behaviors can be derived, in terms of the electrical variables such as the dq-axes currents and the PMSM rotor speed ω_m. Note that the wheel speed ω_w, is simply achieved by the rotor speed from (10). As shown in (10), the rotational torque of the axle shaft T_{as} produces rotational force of the drive wheel, which converts into propulsion forces of the vehicle. The axle shaft torque, which functions as an important factor for vehicle dynamics, can be derived as (19), by substituting (6) and (18) into (10) and (12).

$$\begin{aligned}T_{as} = {} & \frac{3PG_{total}\eta_{total}}{4}\left(1 + \frac{J_{as} - J^*_{total}G_{total}}{R_w^2(m+\Delta m)}\right)\left[\lambda_f i_q + (L_d - L_q)i_d i_q\right] \\ & + \frac{k_{air}R_w\left(J^*_{total}G_{total} - J_{as}\right)}{G_{total}^2(m+\Delta m)}\omega_m^2 + C_{T_{as}}\end{aligned} \quad (19)$$

where, $C_{T_{as}} = \frac{mg(J^*_{total}G_{total} - J_{as})(\sin\phi + \mu_x)}{R_w(m+\Delta m)}$

With a road condition and a vehicle model specified, the C_{Tas} in (19) is decided as a constant value. It is seen from (19) that the torque of the axle shaft T_{as} can be directly coupled to the q-axis current i_q and the rotor speed ω_m, since the d-axis current i_d is generally much smaller than the q-axis current i_q. Using (6), (13), and (18), the tractive force of the vehicle F_x is also expressed with the electrical variables as

$$\begin{aligned}F_x = {} & \frac{3PG_{total}\eta_{total}}{4R_w}\left(1 - \frac{J_{total}G_{total}}{R_w^2(m+\Delta m)}\right)\left[\lambda_f i_q + (L_d - L_q)i_d i_q\right] \\ & + \frac{J_{total}k_{air}}{G_{total}(m+\Delta m)}\omega_m^2 + C_{F_x}\end{aligned} \quad (20)$$

where, $C_{F_x} = \frac{mgJ_{total}G_{total}(\sin\phi + \mu_x)}{R_w^2(m+\Delta m)}$

The C_{Fx} in (20) is also a constant decided by a circumstance of road and a vehicle model. Since the tractive force is closely related with the axle shaft torque, the Eq. (20) is, as expected, similar with (19). The vertical forces on the front and rear wheels, F_{zf} and F_{zr}, are derived as (21) and (22), by substituting (6) and (18) into (14) and (15), respectively.

$$\begin{aligned}F_{zf} = {} & \frac{1}{a_1 + a_2}\left[-\frac{3PhG_{total}\eta_{total}}{4R_w}\left(1 - \frac{J_{total}G_{total}}{R_w^2(m+\Delta m)}\right)\left[\lambda_f i_q + (L_d - L_q)i_d i_q\right]\right. \\ & \left. - \frac{hJ_{total}k_{air}}{G_{total}(m+\Delta m)}\omega_m^2 - hC_{F_x} + C_{F_{zf}}\right]\end{aligned} \quad (21)$$

$$\begin{aligned}F_{zr} = {} & \frac{1}{a_1 + a_2}\left[\frac{3PhG_{total}\eta_{total}}{4R_w}\left(1 - \frac{J_{total}G_{total}}{R_w^2(m+\Delta m)}\right)\left[\lambda_f i_q + (L_d - L_q)i_d i_q\right]\right. \\ & \left. + \frac{hJ_{total}k_{air}}{G_{total}(m+\Delta m)}\omega_m^2 + hC_{F_x} + C_{F_{zr}}\right]\end{aligned} \quad (22)$$

where, $C_{F_{zf}} = a_2 mg\cos\phi$ and $C_{F_{zr}} = a_1 mg\cos\phi$

The vertical force on the rear wheels in (22) can be related with the vertical force on the front wheels in (21) as

$$F_{zr} = F_{zf} + mg\cos\phi \quad (23)$$

From (23), it can be noted that the two vertical forces exhibit the same magnitude and the opposite direction with respect to each other, since the term $mg\cos\phi$ can be, in general, negligible compared to the vertical forces. Thus, the vehicle experiences contrary forces vertically acting on the front and the real wheels, with increasing q-axis current i_q and escalated rotor speed ω_m. The vehicle acceleration a_x in the tractive direction can be expressed as

$$a_x = \frac{1}{m + \Delta m}\left[\frac{3PG_{total}\eta_{total}}{4R_w}\left[\lambda_f i_q + (L_d L_q)i_d i_q\right]\frac{k_{air}R_w^2}{G_{total}^2}\omega_m^2 - C_{a_x}\right] \quad (24)$$

where, $C_{a_x} = mg(\sin\phi + \mu_x)$

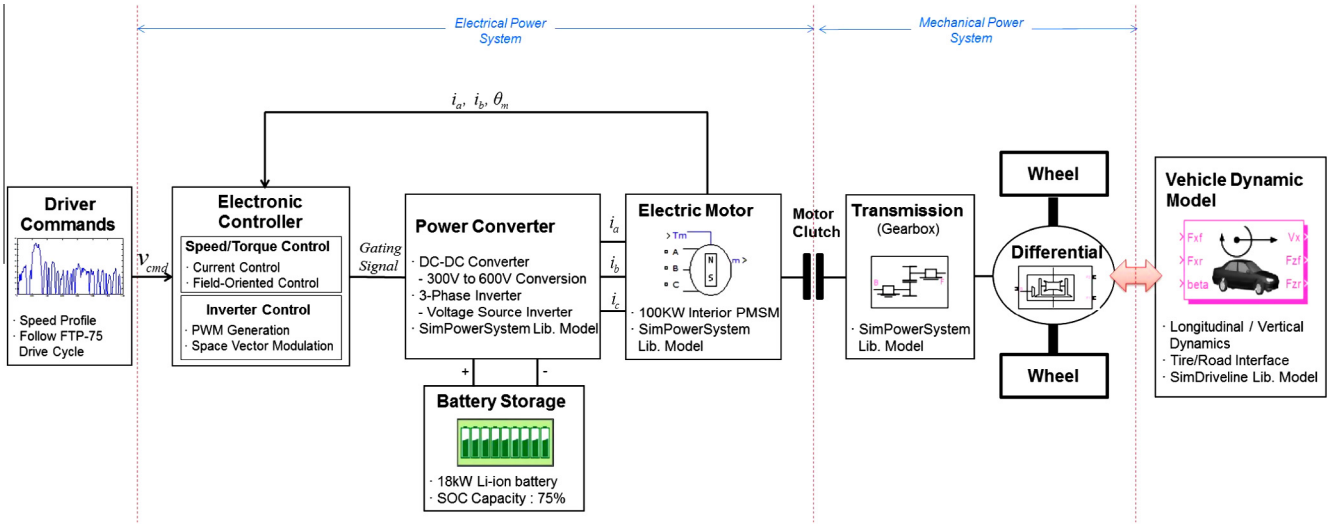

Fig. 4. Overall configuration of EV Matlab model.

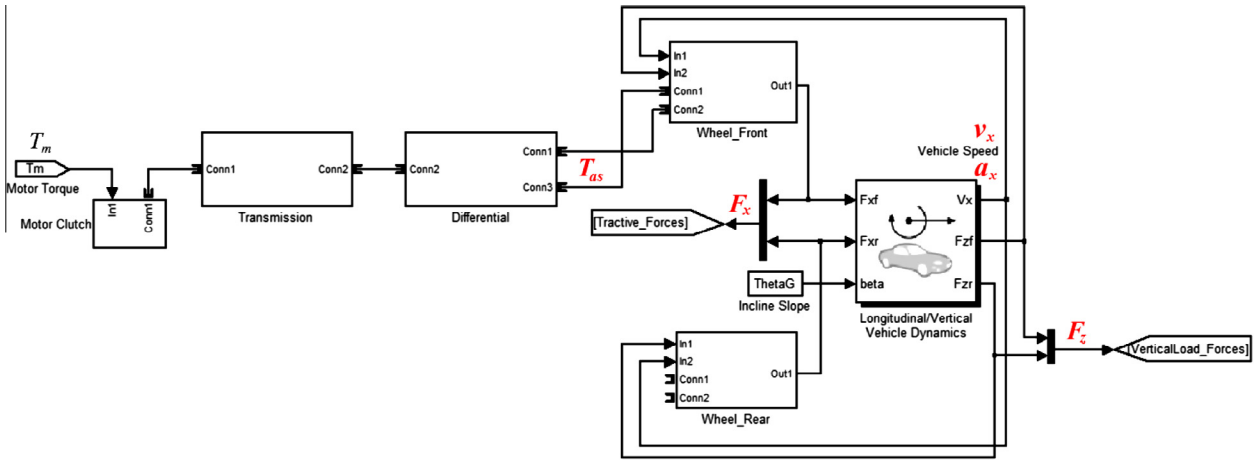

Fig. 5. Schematic model of EV mechanical sub-system with two-wheel longitudinal/vertical dynamics.

Table 2
EV dynamic parameters.

Parameter	Value	Unit
Vehicle mass (m)	1450	kg
Frontal area of the vehicle (A)	2.711	m^2
Wheel radius (R_w)	0.43	m
Coefficient of aerodynamic drag (C_D)	0.29	–
Air density (ρ), at 20 °C	1.204	kg/m^3
Rolling resistance coefficient (μ_x)	0.013	–
Power transmission efficiency (η_{total})	100	%
Total inertia (J_{total})	5.209	$kg\ m^2$
Total gear ratio (G_{total})	8.75	–
Distance from CG to front wheel axle (a_1)	1.4	m
Distance from CG to rear wheel axle (a_2)	1.4	m
Height of CG from the ground (h)	0.5	m

Since the vehicle acceleration is represented by (24), the vehicle speed v_x can be easily obtained by integrating the vehicle acceleration for the total driving time.

In the case where the vehicle operates at low speed, the vehicle dynamics in (19)–(24) can be further simplified. Because the aerodynamic resistance F_{air} is much smaller than the gradient resistance F_{grad} and the rolling resistance F_{roll} at low velocity, the last term with k_{air} in (18) can be ignored (Onoda & Emadi, 2004). Similarly, the product term of k_{air} and ω_m^2 in (19)–(24) can be, at low speed, ignored, resulting in the simplified relationships between the vehicle dynamics and the electrical quantities.

3.2. Matlab models

In this section, an EV Matlab model is developed to verify the theoretical model derived as closed-form expressions in the previous section. The one-motor based EV in Fig. 2 is constructed with reference to components and library models of Matlab/Simulink as well as parameters used in experimental specifications of EVs (Trovao, Pereirinha, & Jorge, 2009). Overall configuration of the EV Matlab model is constructed as shown in Fig. 4. The simulation model is composed of driver commands, electrical sub-system, mechanical sub-system, and vehicle dynamic model. The electrical sub-system, which includes an electronic controller with speed/torque control blocks and a PWM block, battery storage, power converters with the inverter and the DC–DC converter, and a 100 kW PMSM, is developed using the SimPowerSystem library model. In addition, the vehicle dynamic model is designed based on the SimDriveline library model provided by the Simulink/Simscape, to represent longitudinal/vertical dynamic model and tire/road conditions. Fig. 5 shows the constructed Matlab model

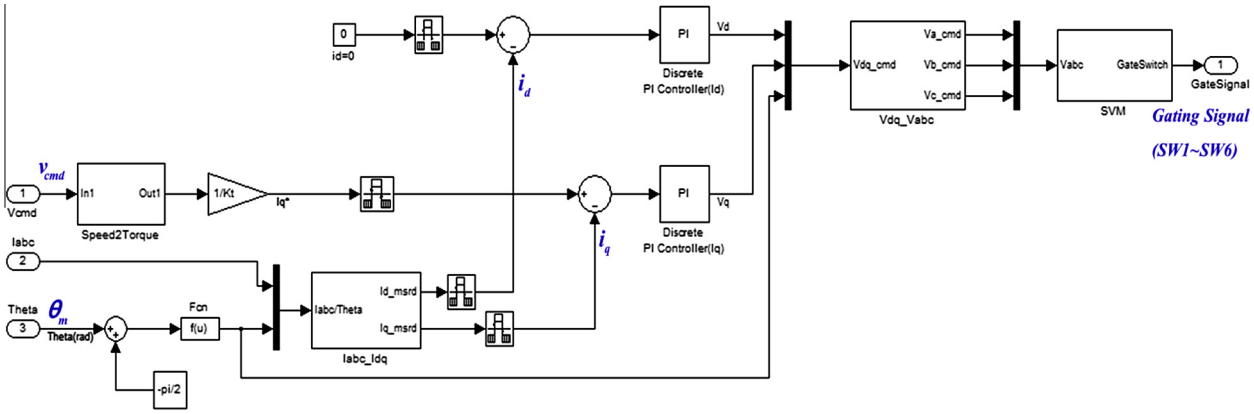

Fig. 6. Schematic model of electronic controller.

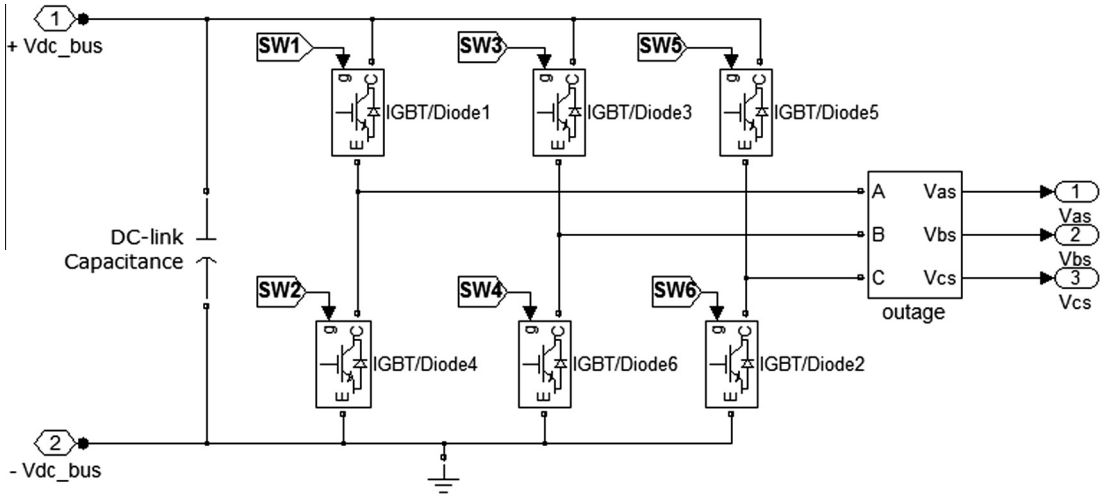

Fig. 7. Schematic model of three-phase inverter.

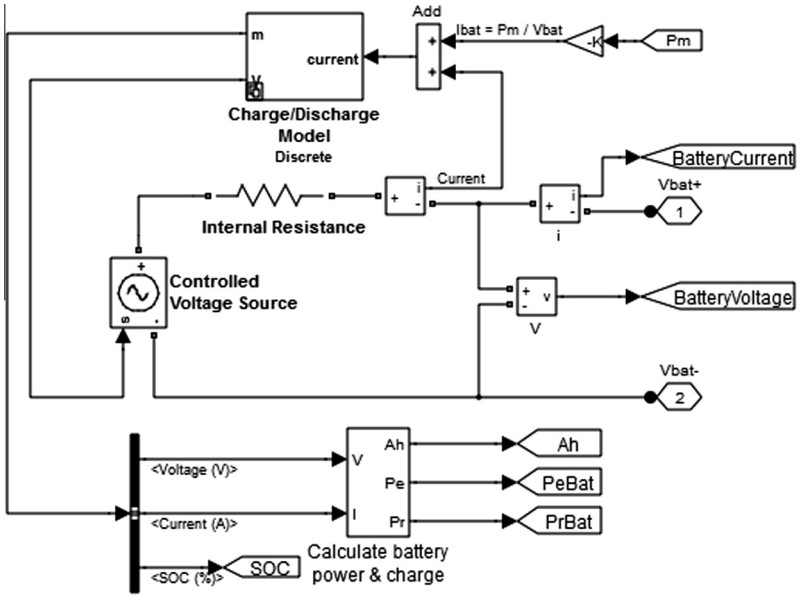

Fig. 8. Schematic model of battery.

Table 3
Battery parameters.

Parameter	Value	Unit
Battery type	Lithium-Ion	–
Nominal voltage	300	V
Rated capacity	50	Ah
Initial state-of-charge (SOC)	75	%

Table 4
Specification of 100 kW PMSM.

Parameter	Value	Unit
d-axis Inductances (L_d)	0.17	mH
q-axis Inductances (L_q)	0.29	mH
Flux linkage (λ_f)	0.071	Wb
Stator-winding resistance (R_s)	0.0083	Ohm
Number of pole (P)	8	–
Moment of inertia (J_m)	0.089	kg m^2
Viscous friction coefficient (B_m)	0.005	Nm/rad/s

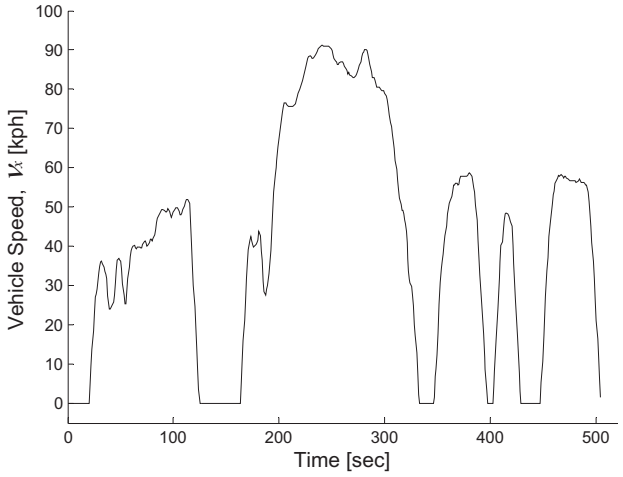

Fig. 9. Coldstart phase of FTP-75 drive cycle.

based mechanical sub-system with two-wheel longitudinal/vertical dynamics using SimDriverline in Simulink toolbox. The front-wheel EV drive equipped with the PMSM as a traction motor is built based on the mechanical structure of propulsion systems in Matlab/Simulink Model. Vehicle parameters provided by demonstration models of Matlab/Simulink are utilized to set the parameters of the EV mechanical structure, such as the vehicle mass, the frontal area of the vehicle, and the wheel radius. On the other hand, the non-structural parameters, including the aerodynamic drag coefficient, the rolling resistance coefficient, the air density, and the power transmission efficiency, are employed with reference to the experimental specifications of EVs (Ehsani et al., 1997; Hayes et al., 2011; Trovao et al., 2009). Table 2 shows the vehicle specifications of the EV Matlab model constructed in this paper.

The Matlab model built for the electronic controller is shown in Fig. 6. An input signal of the electronics controller is the speed profile obtained from driver commands. The controller transforms the speed profile to the corresponding reference motor speed and the motor torque, and then, the reference dq-axes currents are produces by the vector control for the PMSM. The actual dq-axes currents, achieved by the abc-dq transformation of the three-phase inverter output currents, are regulated by the PI current controllers. In order to generate three-phase sinusoidal currents with variable frequency and variable amplitude from the dc voltage, a PWM voltage source inverter is, as shown in Fig. 7, realized with the discrete insulated-gate bipolar transistors (IGBTs) and the capacitor, which are provided with the SimPowerSystem library. The space vector PWM algorithm is utilized to generate the gate signals of the three-phase inverter, which drives the PMSM (Emadi, 2005; Kwak, Kim, & Park, 2010). The inverter output voltage directly depends on the ON/OFF states of the inverter gate input. The DC–DC bidirectional converter is utilized to convert the 300 V battery voltage to 600 V dc-link voltage.

Regarding the battery block realized with the Matlab/Simulink, the Battery block is implemented as a generic dynamic model with rechargeable Li-ion battery, which is currently being applied to many eco-friendly vehicles. The equivalent circuit of the battery realized in this paper, using the generic battery block in SimPowerSystem, is shown in Fig. 8. A battery is modeled as a controlled voltage source and an internal resistance, which are changed with the electric power flow and load. The charge/discharge model block calculates the present battery voltage as a function of battery state-of-charge (SOC), and then, calculates the output current. The battery storage part in the Matlab model employs a Li-ion battery with parameter illustrated in Table 3. The battery initial configuration was set to 75% SOC with 300 V nominal voltages, since the generic battery maintains the SOC between 40% and 80% in the normal mode. The 100 kW PMSM as the traction motor is implemented from the motor library model of SimPowerSystem, where the specification of PMSM is represented in Table 4.

3.3. Verification of analytic model with Matlab model

To verify the theoretical models, represented by (19)–(24), as the closed-form numerical expressions, the vehicle dynamics obtained from the theoretical models are compared with those

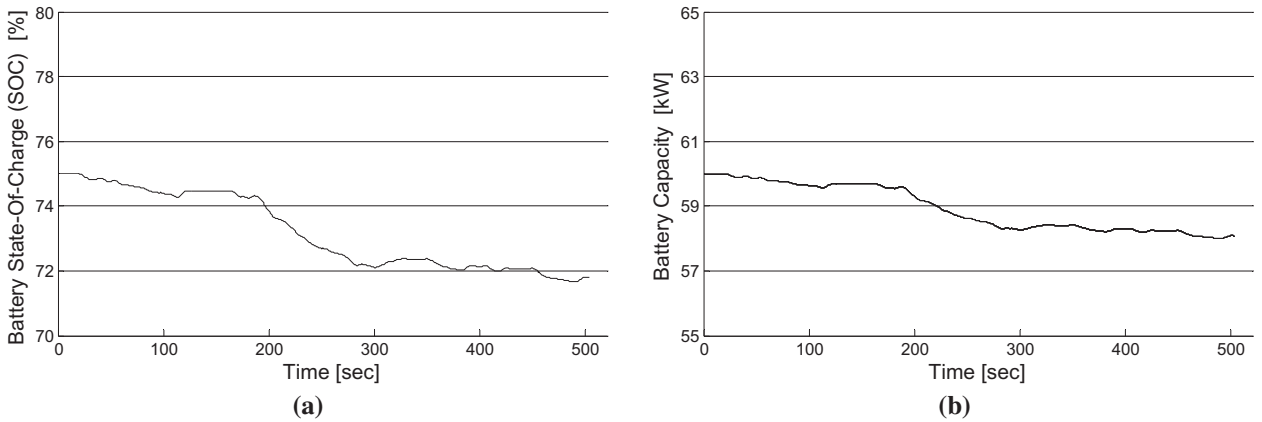

Fig. 10. Battery characteristics with FTP-75 drive cycle.

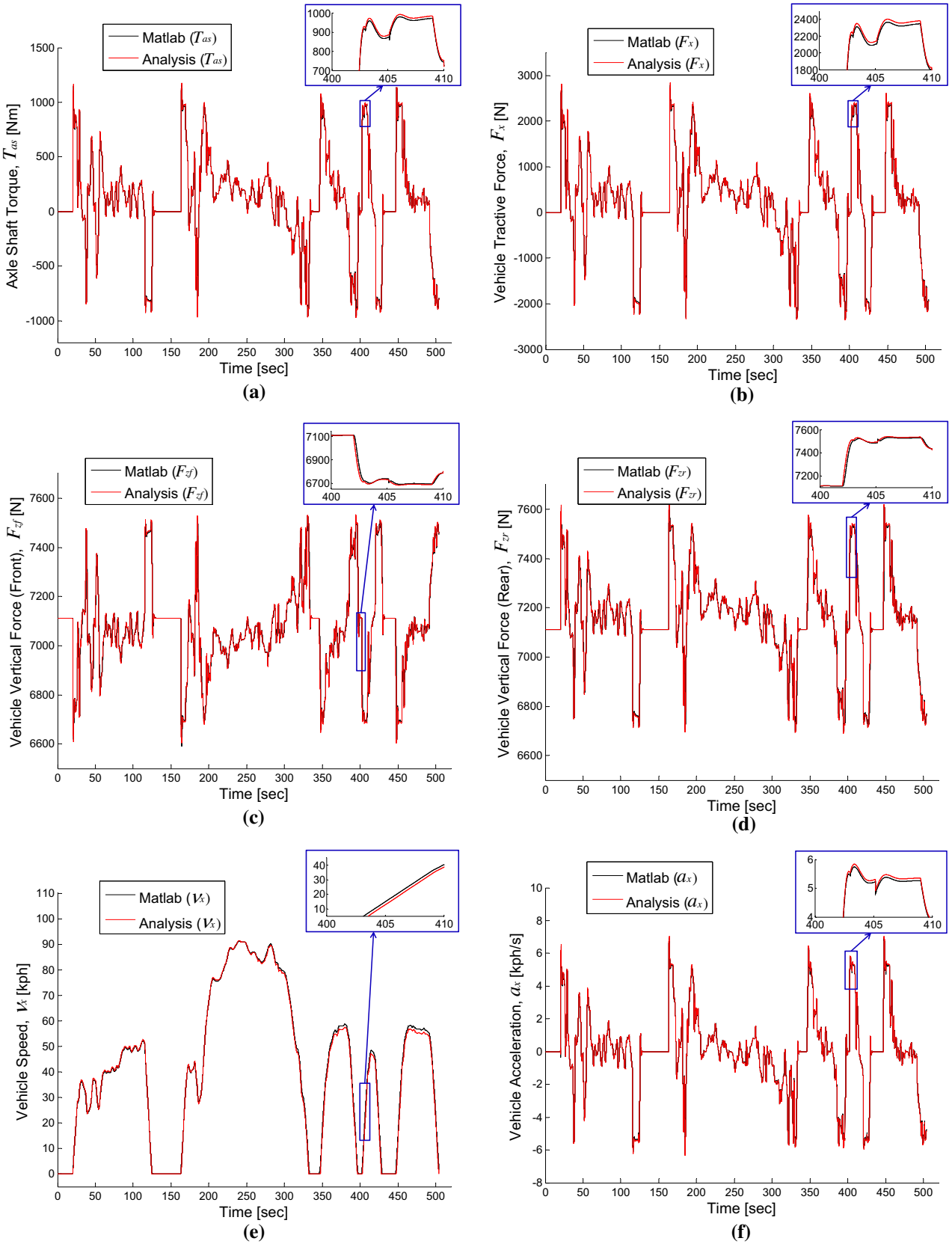

Fig. 11. Comparisons of vehicle dynamics obtained from analytic model and Matlab based model with FTP-75 drive cycle.

resulted from the Matlab based model. The Federal Test Procedure-75 (FTP-75) of the environmental protection agency (EPA) is employed for the speed profile, because it has been commonly used for the performance test of general city driving. The FTP-75 consists of three driving phases with various acceleration and deceleration regions, such as cold start phase, transient phase, and hot

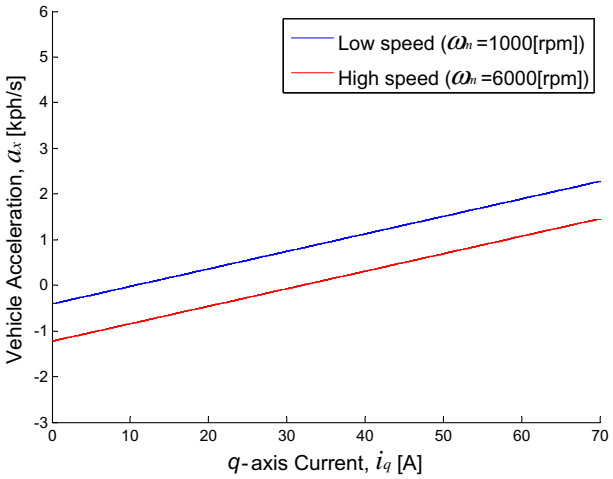

Fig. 12. Vehicle acceleration versus q-axis current.

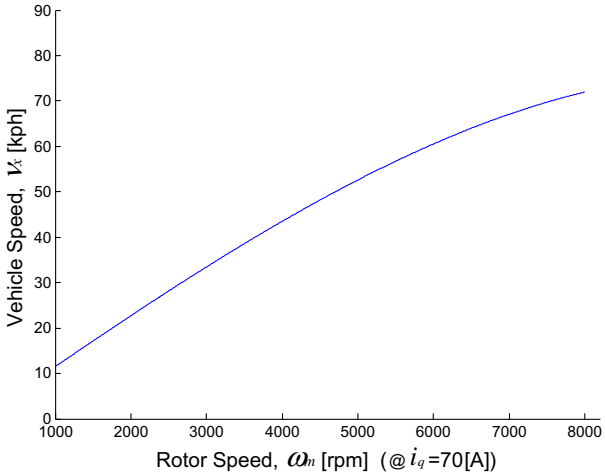

Fig. 14. Vehicle speed as a function of rotor speed.

start phase. In this verification, the cold start phase, lasting for 505 s, is used as shown in Fig. 9. In the Matlab model, the sampling period of controller and the switch frequency of inverter are set to 50 μs and 5 kHz, respectively. Since the analytic model starts from the inverter output currents in the dq-axes, the dq-axes currents obtained by the FTP-75 drive cycle in the Matlab based model are utilized for the inputs of the theoretical model.

Fig. 10 illustrates the traces for battery characteristics with the FTP-75 drive cycle. From the Fig. 10, it is seen that the state of charge (SOC) is reduced to approximately 3.5% of its initial value, after the vehicle drives the FTP-75 cycle for 505 s. In addition, the battery capacitor is decreased by 2 kW by maintaining the battery terminal voltage at its nominal value. Fig. 11 shows the results of the vehicle dynamics obtained from both the mathematical analysis model and the Matlab based model. It is clearly shown that all the vehicle dynamic outputs, T_{as}, F_x, F_{zr}, F_{zf}, v_x, and a_x, resulting from the analysis models coincides well with those from the Matlab based model. Fig. 11(a) shows the axle shaft torques resulted from the vehicle speed profile of Fig. 9. For entire speed profile with FTP-75 drive cycle, the results obtained from the analytic axle shaft torque in (19) match those from the Matlab based model. Fig. 11(b) illustrates the vehicle tractive forces generated by the speed profile v_{cmd}. The waveform of the mathematical analysis model is achieved by (20), which conforms to the results from the Matlab model. The vehicle tractive force F_x is analogous to the axle shaft torque of Fig. 11(a). This is due to the fact that the vehicle tractive force F_x is proportional to the wheel torque T_w, which is determined by the axle shaft torque T_{as} in (10). The vehicle vertical forces on the front wheels, obtained the analytic model of (21) as well as the Matlab based model, are demonstrated in Fig. 11(c), where the two results coincide well. It is shown that the vertical force on the front wheel F_{zf} of Fig. 11(c) shows the waveforms shifted by 7112 [N] and turned upside down at the center of 7112 [N], compared to the tractive force F_x of Fig. 11(a), which is obvious from the mechanical behavior models of (13) and (14) as well as parameters in Table 2. The curves of Fig. 11(d) depict the vehicle vertical forces on the rear wheels from the mathematical analysis model of (22) and the Matlab based model, which are almost identical. Obviously seen from Fig. 11(c) and (d), the two vertical forces on the front and the rear wheels show the waveforms turned upside down at the center of 7112 [N], as expected in (21)–(23). Fig. 11(e) demonstrates the vehicle speeds in the tractive direction v_x resulted in the analytic model obtained by integrating (24) and the Matlab based model. It is clear that the tractive speeds v_x resulted from both the analytic and the Matlab based model are consistent with the speed profile v_{cmd} by

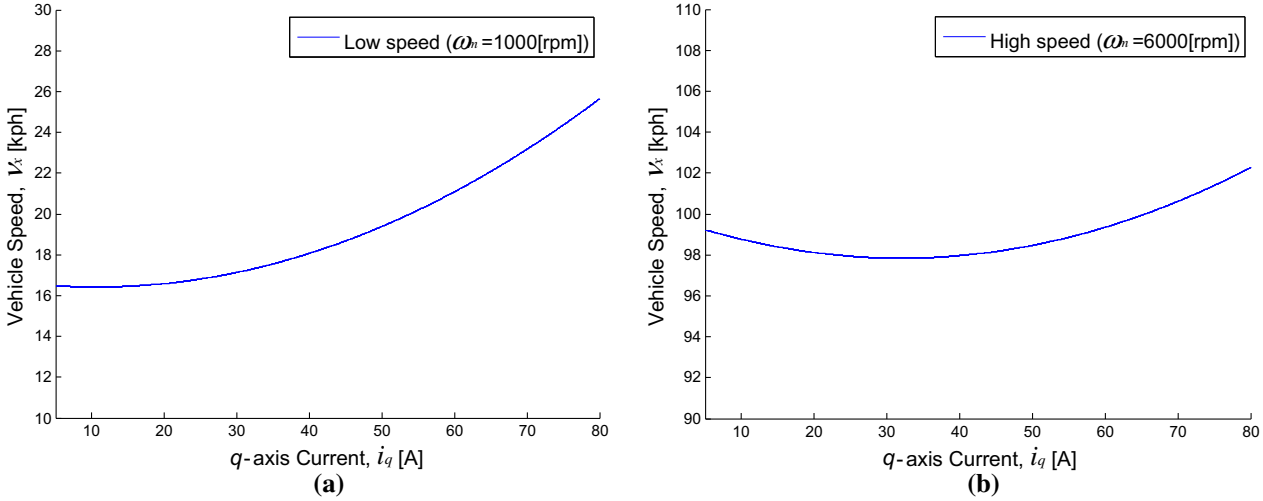

Fig. 13. Vehicle speed as a function of q-axis current.

the FTP-75 drive cycle of Fig. 9. Fig. 11(f) depicts the waveforms of the vehicle acceleration in the tractive direction, obtained from the analytic model of (24) and the Matlab based model.

Thus, all the mathematical closed-form expressions based on the derived analytic models in (19)–(24) are, for the standard speed profile of the FTP-75 drive cycle, consistent with the results obtained from the Matlab based model. As a result, it can be concluded that the developed numerical analysis models can be used to predict the vehicle dynamic behaviors T_{as}, F_x, F_{zr}, F_{zf}, v_x, and a_x, from the electrical quantities, including the dq-axes inverter output currents and the rotor speed. Therefore, the proposed modeling the entire EV powertrains has such the advantages as: (1) the analytic model developed in this paper permits much faster execution time even with the high resolution to achieve accurate analysis results about dynamic behaviors of the EV. (2) The developed analytic model of the EV powertrain based on the mathematical equations can be utilized to easily obtain input and output EV data by using simple computational software such as Microsoft Excel, regardless of specific simulation software platforms, such as Matlab, dSPACE, and AMESim. (3) The model designer can handles all of EV parameters and variables in the analytic model, and then it has a high flexibility and applicability to implement desired models, in contrast to conventional Matlab based model where the kernel models are predefined with fixed libraries with no modifications by designers. On the other hand, the developed EV analysis model is based on the normal balanced three-phase systems, assuming that $i_a + i_b + i_c = 0$. Thus, this model is only applicable in the electrical normal state and it does not take into account an abnormal state, such as open/short failures of switches in the inverter, which is a disadvantage of this analytic model. The authors plan to expand the research scope into the abnormal modes based on theoretical analysis in the future.

4. Analysis of relationship between electrical variables and vehicle dynamics

In this section, the correlation between the electric input signals and the mechanical final output variables is presented by graphs and analytic descriptions based on the derived theoretical analysis. From the correlation discovered in this section, final EV dynamics, such as the wheel speed, the wheel torque, the vertical forces on front and rear wheel, the tractive force, and the speed/acceleration in the vehicle tractive direction, can be easily monitored and predicted using the proposed analysis models and the real-time electric signals.

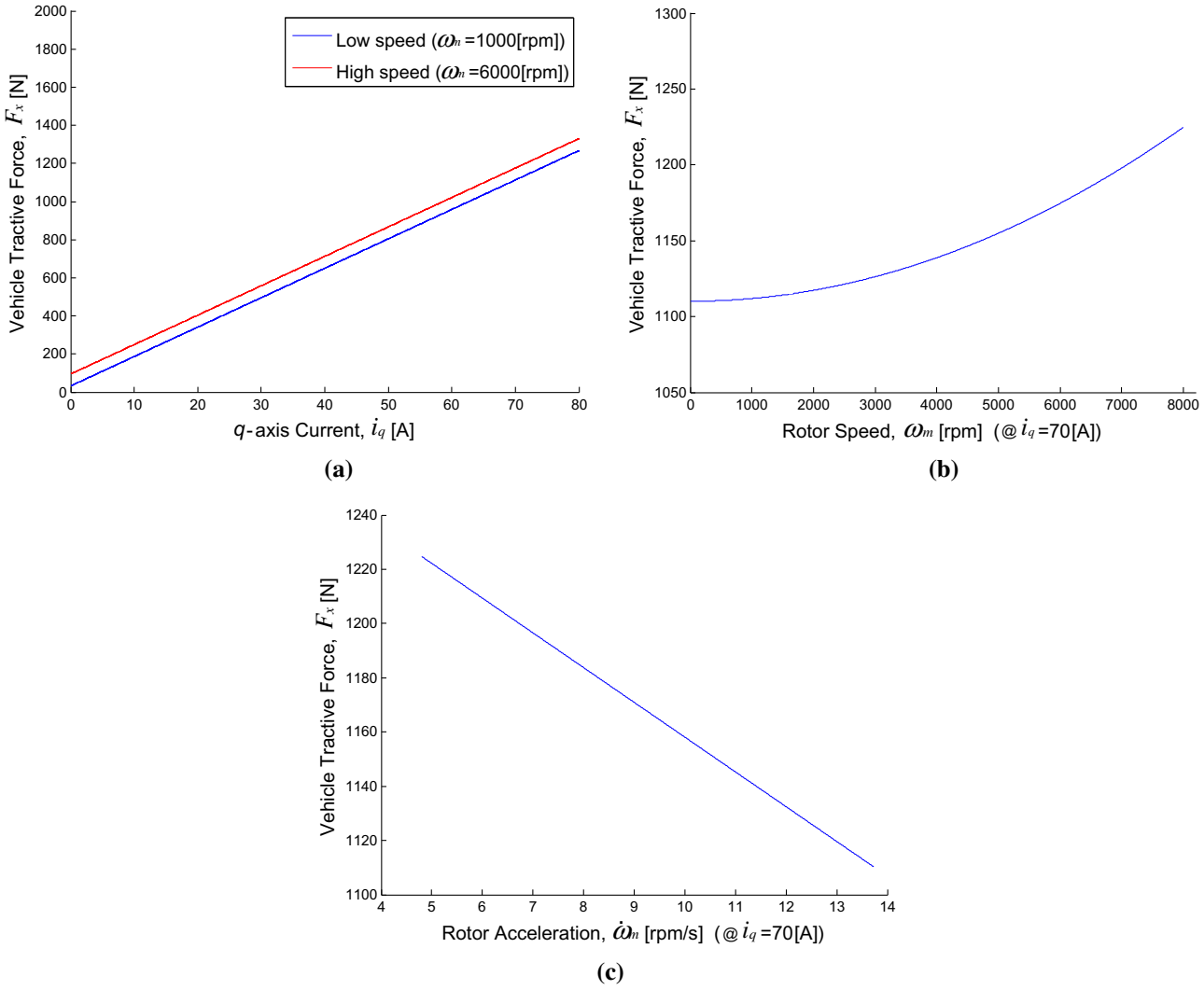

Fig. 15. Vehicle tractive forces versus (a) q-axis current (b) rotor speed (c) rotor acceleration.

A variety of influences of the q-axis current and the rotor speed on the vehicle dynamics are investigated based on (19)–(24). For the high-speed operating region corresponds to the flux weakening region of the PMSM with a small negative d-axis current ($|i_d| > 0$) component to extend the operating regions of the PMSM. Although three-dimensional curves of the vehicle dynamics as function of the current i_q and the rotor speed ω_m are more feasible from physics point of view, two-dimensional figures are, in this paper, illustrated for the purpose of distinct display. Fig. 12 shows the vehicle acceleration as a function of the q-axis current obtained from (24), assuming that a rotor speed is fixed to a constant value at 1000 and 6000 rpm, respectively. It is seen that the vehicle acceleration linearly increases with the increasing magnitude of the q-axis current. It should be noted that the vehicle acceleration shows a negative offset value, in regions where the current i_q is low. This is because the former positive acceleration term generated by the i_q is, in (24), smaller than the two latter negative terms, which are produced by the vehicle inertia, rolling resistance, and aerodynamic resistance. This implies that the vehicle can be accelerated when the current i_q increases enough to compensate for the negative acceleration terms representing the inertia and the driving resistances.

Fig. 13 shows the vehicle speed in the tractive direction as a function of the q-axis current obtained by integrating (24). Fig. 13(a) illustrates that the vehicle speed v_x gradually increases as the torque component current i_q increases, with constant rotor speeds at 1000 rpm. It is recognized, from Fig. 13(a), that the vehicle speed operated with low currents slightly reduces from its initial speed, due to the negative value of the acceleration with low i_q in (24). The vehicle speed with ω_m set to 6000 rpm versus the i_q is presented in Fig. 13(b). It is seen that the vehicle speed with low i_q in Fig. 13(b) reduces more from its starting value than that in Fig. 13(a), because the negative term with ω_m^2 in (24) increases. The vehicle speed in the tractive direction as a function of the rotor speed is shown in Fig. 14 with constant current i_q. The vehicle speed v_x increases nearly linearly with the increasing rotor speed. It is observed that the slope of the vehicle speed gradually decreases, as the vehicle runs at high speed with increasing rotor speed. This is due to the fact that the aerodynamic resistance term with k_{air} in (24), which is proportional to ω_m^2, prevents the vehicle speed v_x from linearly increasing with ω_m. Therefore, the vehicle speed in the tractive direction slightly decreases in a high-speed region, because of rapidly increasing aerodynamic resistance. This reduction of the vehicle speed can be compensated by increasing the q-axis current with the increasing vehicle speed.

The vehicle tractive forces obtained from (20), as a function of the q-axis current and the rotor speed, are shown in Fig. 15. It is seen from Fig. 15(a) that the tractive force is linearly dependent on the q-axis current with constant rotor speeds. Fig. 15(b) shows the quadratic relationship between the rotor speed and the tractive

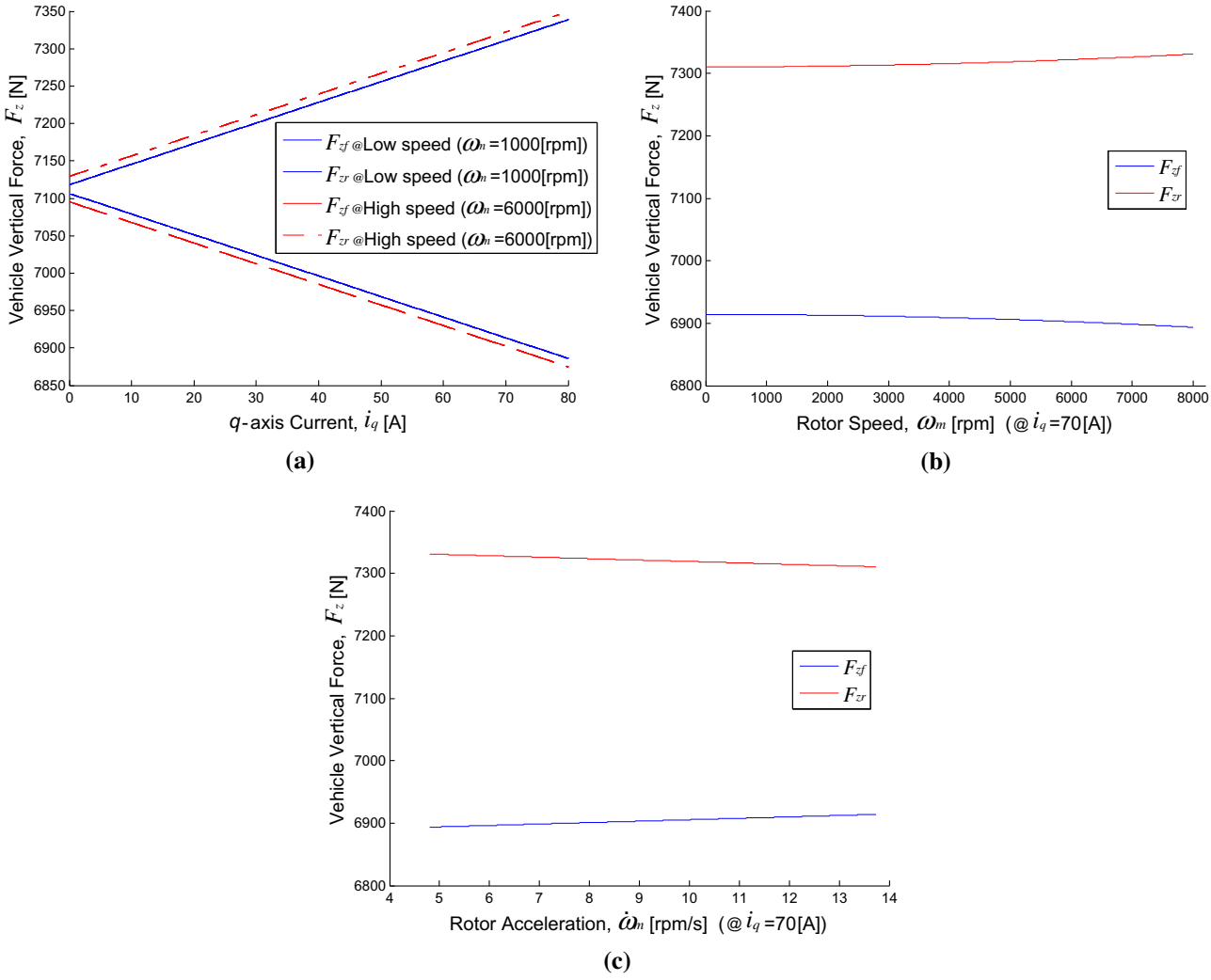

Fig. 16. Vehicle vertical forces as a function of (a) q-axis current (b) rotor speed (c) rotor acceleration.

force with a constant q-axis current, as is obvious from (20). From (13), the resistance force associated with the total inertia J_{total} increases according to the increase in the rotor acceleration. Thus, the vehicle tractive force F_x reduces with increasing rotor acceleration, in case that the torque component current i_q set to the constant value, as shown in Fig. 15(c).

Fig. 16 illustrates the influences on the vehicle vertical forces of the current i_q, the rotor speed, and acceleration. Fig. 16(a) shows the vehicle vertical forces as a function of the q-axis current for constant rotor speeds. It is seen that the vertical force on the front wheels F_{zf} linearly increases with the increasing torque component current. On the contrary, the vertical force on the rear wheels F_{zr} reduces as much as the force F_{zf} increases, as expected from (21) and (22). As a result, the difference between the vertical forces on the front and rear wheels increases with increasing q-axis current, as shown in Fig. 16(a). Likewise, from (21) and (22), the rotor speed changes the vertical forces on the front and rear wheels with the same magnitude and opposite direction. It can be seen from Fig. 16(b) that the forces F_{zf} and F_{zr} increase and decrease with symmetry quadratic curves, respectively, with increasing rotor speed, in the case of constant q-axis current. Therefore, high torque and high speed operation of the vehicle can result in unstable operating condition from standpoints of the vertical behavior of the vehicle, due to increased deviation between the two vertical forces. Fig. 16(c) represents the relationship between the rotor acceleration and vertical forces of the vehicle. From (14) and (15), the vertical forces of the front and rear wheels, F_{zf} and F_{zr}, increases and decreases with increasing rotor acceleration, respectively. In contrast to the rotor speed, increasing rotor acceleration gradually reduces the variation between the two vertical forces.

5. Conclusion

In this paper, the entire analysis model for the powertrain of EVs has been developed, based on mathematical approaches, to describe the EV dynamics with respect to electrical quantities, in consideration of both mechanical and electrical sub-systems. The vehicle dynamic behaviors, such as the acceleration, the speed, the tractive forces, and vertical forces of the EV, have been derived as the closed-form expressions, in terms of the inverter output currents and the rotor speed of the PMSM of the electrical sub-system. The theoretical analysis models have been validated, by comparison with the simulation model developed with the Matlab/Simulink platform, by testing with the FTP-75 drive cycle. Based on theoretical analysis of the EV powertrain, various influences on the vehicle dynamics have been investigated and analyzed with respect to the electrical quantities.

Acknowledgments

This Research was supported by Basic Science Research Program through the National Research Foundation of Korea (NRF) funded by the Ministry of Education, Science and Technology (2011-0013884) and the DGIST R&D Program of the Ministry of Science, ICT and Future Planning of Korea (13-RS-03).

References

Butler, K. L., Ehsani, M., & Kamath, P. (1999). A Matlab-based modeling and simulation package for electric and hybrid electric vehicle design. *IEEE Transactions on Vehicular Technology, 48*, 1770–1778.

Chan, C. C. (2002). The state of the art of electric and hybrid vehicles. *Proceedings of the IEEE, 90*, 247–275.

Ehsani, M., Rahman, K. M., & Toliyat, H. A. (1997). Propulsion system design of electric and hybrid vehicles. *IEEE Transactions on Industry Applications, 44*, 19–27.

Emadi, A. (2005). *Handbook of automotive power electronics and motor drives* (1st ed.). New York: CRC Press (Chapter 5).

Fujii, K., & Fujimoto, H. (2007). Traction control based on slip ratio estimation without detecting vehicle speed for electric vehicle. In *Power conversion conference* (pp. 688–693).

Gao, D. W., Mi, C., & Emadi, A. (2007). Modeling and simulation of electric and hybrid vehicles. *Proceedings of the IEEE, 95*, 729–745.

García, P., Torreglosa, J. P., Fernández, L. M., & Jurado, F. (2013). Control strategies for high-power electric vehicles powered by hydrogen fuel cell, battery and supercapacitor. *Expert Systems with Applications, 40*, 4791–4804.

Hayes, J. G., Oliveira, R. P. R., Vaughan, S., & Egan, M. G. (2011). Simplified electric vehicle power train models and range estimation. In *Vehicle power and propulsion (VPPC'11 IEEE)* (pp. 1–5).

Jazar, R. N. (2008). *Vehicle dynamics: Theory and application* (1st ed.). New York: Springer (Chapter 2).

Kroeze, R. C., & Krein, P. T. (2008). Electrical battery model for use in dynamic electric vehicle simulations. In *Power electronics specialists conference (PESC'08 IEEE)* (pp. 1336–1342).

Kwak, S. (2012). Four-leg based fault-tolerant matrix converter schemes based on switching function and space vector methods. *IEEE Transactions on Industrial Electronics, 59*, 235–243.

Kwak, S., Kim, T., & Park, G. (2010). Phase-redundant based reliable direct ac/ac converter drive for series hybrid off-highway heavy electric vehicles. *IEEE Transactions on Vehicular Technology, 59*, 2674–2688.

Mapelli, F. L., Tarsitano, D., & Mauri, M. (2010). Plug-in hybrid vehicle: Modeling, prototype realization, and inverter losses reduction analysis. *IEEE Transactions on Industrial Electronics, 57*, 598–607.

Mohan, N., Underland, T. M., & Robbins, W. P. (1995). *Power electronics* (2nd ed.). New York: Wiley (Chapter 8).

Murakami, H., Kataoka, H., Honda, Y., Morimoto, S., & Takeda, Y. (2001). Highly efficient brushless motor design for an air-conditioner of the next generation 42 V vehicle. In *Industry application society annual meeting (IAS'01 IEEE)* (pp. 461–466).

Na, W., Park, T., Kim, T., & Kwak, S. (2011). Light fuel-cell hybrid electric vehicles based on predictive controllers. *IEEE Transactions on Vehicular Technology, 60*, 89–97.

Nair, A., & Rajagopal, K. R. (2010). Generic model of an electric vehicle for dynamic simulation and performance prediction. In *Conference of electrical machines and systems* (pp. 753–757).

Onoda, S., & Emadi, A. (2004). PSIM-based modeling of automotive power systems: Conventional, electric, and hybrid electric vehicles. *IEEE Transactions on Vehicular Technology, 53*, 390–400.

Powell, B. K., Bailey, K. E., & Cikanek, S. R. (1998). Dynamic modeling and control of hybrid electric vehicle powertrain systems. *IEEE Transactions on Control System Technology, 18*, 17–33.

Trovao, J. P., Pereirinha, P. G., & Jorge, H. M. (2009). Design methodology of energy storage systems for a small electric vehicle. In *International battery, hybrid and fuel cell electric vehicle symposium* (pp. 1–12).

Yin, D., Oh, S., & Hori, Y. (2009). A novel traction control for EV based on maximum transmissible torque estimation. *IEEE Transactions on Industrial Electronics, 56*, 2086–2094.